BIOCHEMISTRY

A thrombin-triggered self-regulating anticoagulant strategy combined with anti-inflammatory capacity for blood-contacting implants

Yanan Wang[1], Haoshuang Wu[1], Zhongyi Zhou[1], Manfred F. Maitz[2,3], Kunpeng Liu[1], Bo Zhang[1], Li Yang[1], Rifang Luo[1]*, Yunbing Wang[1]*

Interrelated coagulation and inflammation are impediments to endothelialization, a prerequisite for the long-term function of cardiovascular materials. Here, we proposed a self-regulating anticoagulant coating strategy combined with anti-inflammatory capacity, which consisted of thrombin-responsive nanogels with anticoagulant and anti-inflammatory components. As an anticoagulant, rivaroxaban was encapsulated in nanogels cross-linked by thrombin-cleavable peptide and released upon the trigger of environmental thrombin, blocking the further coagulation cascade. The superoxide dismutase mimetic Tempol imparted the antioxidant property. Polyphenol epigallocatechin gallate (EGCG), in addition to its anti-inflammatory function in synergy with Tempol, also acted as a weak cross-linker to stabilize the coating. The effectiveness and versatility of this coating were validated using two typical cardiovascular devices as models, biological valves and vascular stents. It was demonstrated that the coating worked as a precise strategy to resist coagulation and inflammation, escorted reendothelialization on the cardiovascular devices, and provided a new perspective for designing endothelium-like functional coatings.

INTRODUCTION

Cardiovascular disease (CVD), including coronary atherosclerotic heart disease and valvular heart disease, has the highest mortality rate among noncommunicable diseases and increases incidence (*1*). As interventional cardiology has developed by leaps and bounds, implantable cardiovascular devices play a vital role in the treatment of CVD (*2*, *3*). High thrombosis risk, however, remains a stumbling block to the effectiveness of cardiovascular implant materials. Coagulation response affects the endothelial process, exacerbates the inflammatory response, and induces late thrombosis (*4*, *5*). Moreover, during interventional procedures, the unavoidable tissue injury damages the endothelial layer, causing host inflammatory and wound healing responses, which are responsible for delayed endothelialization and intimal hyperplasia related to excessive proliferation of smooth muscle cells (SMCs). Coagulation and inflammation even cause calcification, degradation, and restenosis. There are myriad reasons for the failure of cardiovascular implant devices. Chief among them are poor endothelialization and hyperplasia (*6*, *7*). Rapid and healthy reendothelialization of the surface and inhibited hyperplasia, therefore, are the accepted direction for functional modification of cardiovascular blood-contacting devices. Suppressing coagulation and inflammation, as the critical trigger of poor endothelialization and hyperplasia, is an essential entry point to improve the performance of cardiovascular implant materials.

Upon contact with foreign materials, the coagulation reactions are immediately initiated. In the subsequent expansion stage, prothrombin is converted to thrombin and then fibrinogen is converted to fibrin, leading to the eventual formation of clots (*8*). To restrain the coagulation after the contact of biomaterials with blood, various anticoagulant substances have been applied on the blood-contacting surfaces (*9*), such as anti-adhesive macromolecules (*10*, *11*), heparin (*7*), and nitric oxide (NO)–releasing coatings (*12*, *13*). The working mode of most strategies is open-loop, based on passive diffusion and enzymatic activity, with no feedback regulation. Because of the amplifying effect of the rapid coagulation reaction, the optimum/only choice to ensure long-lasting efficacy and match the actual coagulation level is to enhance the amount of substance modification or prolong the service time. However, higher dosage is associated with many potentially harmful side effects, such as bleeding risks (for heparin) (*14*), toxicity (for NO) (*15*), or preterm exhaustion.

The vascular endothelium, which plays a role in regulating the coagulation response physiologically, can provide much biomimetic inspiration for blood-contacting material surface modification. In particular, thrombomodulin on the surface of endothelial cells turns the procoagulant activity of thrombin to an anticoagulant by forming a complex with thrombin, which activates protein C to activated protein C (APC). APC inactivates the coagulation cofactors FVa and FVIIa, thus inhibiting further thrombin generation (*16*). This self-controlled feedback strategy is a paradigm for hemocompatible surface modifications of biomedical devices (*16*–*20*). Thrombin-responsive feedback-controlled drug delivery systems have been used for anticoagulant regulation of the heparin-releasing hydrogel coating, heparin-releasing hydrogel, and nanoparticle loaded with fibrinolysis activator t-PA (tissue plasminogen activator) (*16*, *17*, *20*, *21*). Those works demonstrated that the feedback system rapidly counteracted the coagulation response and performed great potential as an anticoagulant coating. However, current systems are designed for a single anticoagulant purpose and are not combined with other functions, which leads to their inability to meet the multifunctional requirements (anti-hyperplasia, anti-inflammation, pro-endothelialization, etc.) of cardiovascular materials.

The coagulation and inflammatory responses after biomaterial implantation are so closely related that they trigger and worsen each

[1]National Engineering Research Center for Biomaterials, Sichuan University, Chengdu 610064, China. [2]Leibniz Institute of Polymer Research Dresden, Max Bergmann Center of Biomaterials Dresden, Dresden 01069, Germany. [3]Key Laboratory for Advanced Technologies of Materials, Ministry of Education, School of Material Science and Engineering, Southwest Jiaotong University, Chengdu 610031, China. *Corresponding author. Email: lrifang@scu.edu.cn (R.L.); yunbing.wang@scu.edu.cn (Yunbing Wang)

other (*6*, *22*, *23*). The intervention in the inflammation during the process of endothelialization, especially in the early stage, has a positive effect on reendothelialization. The most critical and versatile approach for suppressing the inflammatory response and triggering an appropriate immune response remains inhibition of key signaling molecules in the progression of inflammation. As a target of inflammation treatment, overexpressed reactive oxygen species (ROS) around blood-contacting surface leads to enhanced host defense, increased classically activated macrophages, nuclear factor κB (NF-κB) activation, and biomolecular damage (*24*). Coating with the ability to eliminate ROS or free radicals has proven to be a reasonable and useful strategy to suppress inflammation and other issues induced by inflammation in cardiovascular implantable devices (*25*, *26*). Various antioxidants like ascorbic acid (*27*), antioxidant enzymes (*28*), and glutathione (*29*) have been investigated. However, some of them are limited by high price or low possibility for modification. Since a single function is not sufficient for blood-contacting materials, the anti-inflammatory modification should take into account the combination of anti-inflammatory substances with other functions, especially anticoagulant function. Substances that can interact with other functional molecules without compromising antioxidant activity, such as polyphenols (*7*, *30*) and anti–free radical moieties (*31*), are preferred.

Considering this, a self-regulating anticoagulant strategy combined with anti-inflammatory capacity was proposed. In the early post-implantation period without the coverage of normal endothelium, this coating was expected to mimic part of the thrombomodulin to exercise the anticoagulant function, which was inspired by the thrombin-triggered function and self-controlled feedback of thrombomodulin. As shown in Fig. 1, the functional coating consists of the following

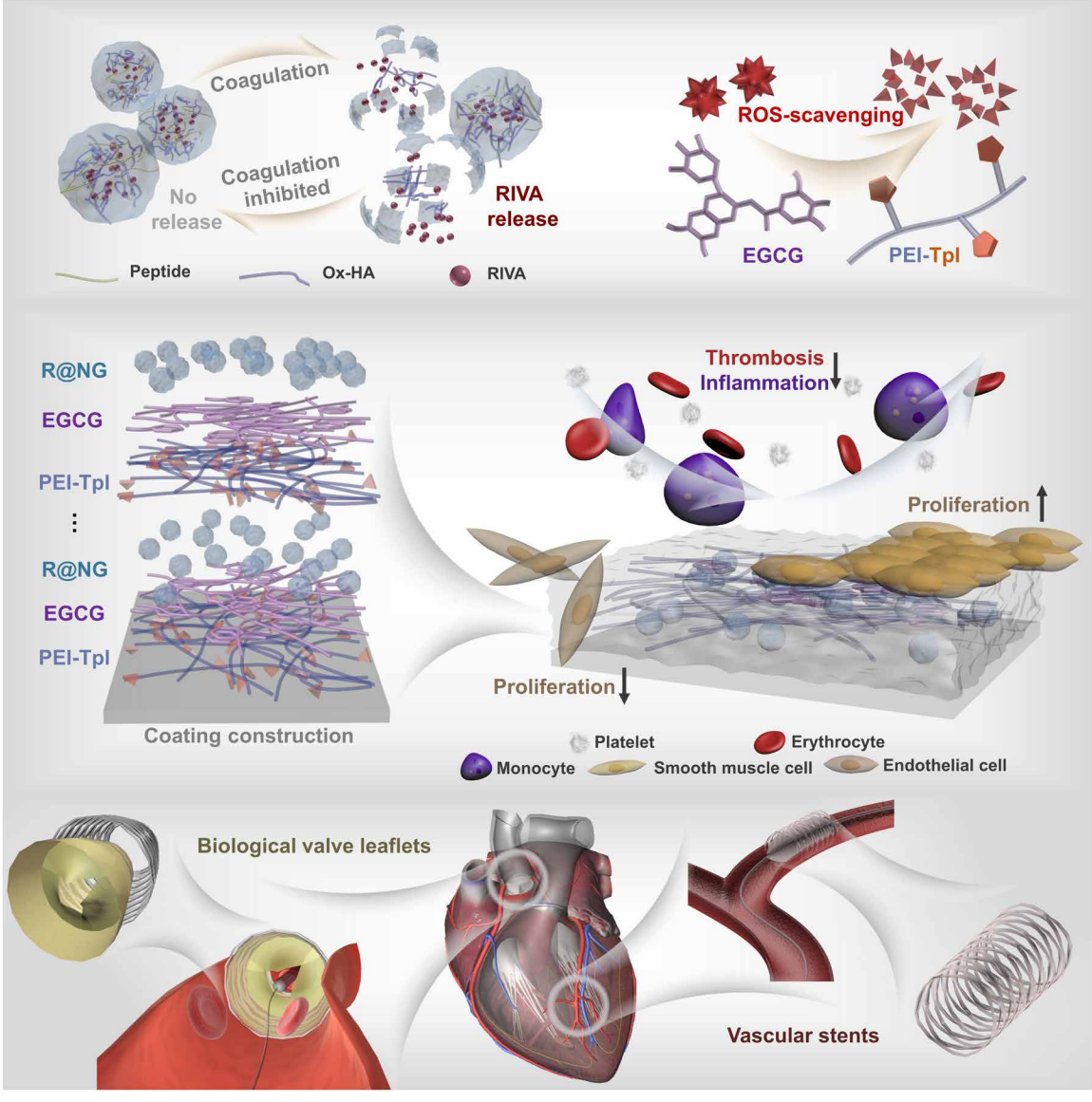

Fig. 1. The functional model and preparation process of the thrombin-triggered anticoagulant strategy combined with anti-inflammatory capacity for blood-contacting implants. Ox-HA, oxidized hyaluronic acid; RIVA, rivaroxaban; EGCG, epigallocatechin gallate; PEI-Tpl, Tempol-grafted polyethylenimine; R@NG, nanogels loaded with RIVA.

modules: (i) self-regulating antithrombotic system realized by thrombin-sensitive nanogels loaded with an anticoagulant. Triggered by environmental thrombin, the nanogels, based on oxidized hyaluronic acid (Ox-HA) with thrombin-cleavable peptide cross-linkers, rapidly released the factor Xa (FXa) inhibitor rivaroxaban (RIVA) (*32*), blocking the coagulation cascade. The level of coagulation activity directly affected the anticoagulant release of the coating, comparable to the feedback-controlled effect of the endothelium. (ii) The second module is the anti-inflammatory system with the ability to scavenge free radicals. Tempol (Tpl), a small radical scavenger with superoxide dismutase–like activity, served as one of the anti-inflammatory modules. Tpl is effective against oxidative stress–related diseases and can be easily grafted on polyanionic polyethylenimine (PEI) (PEI-Tpl) to participate in a coating assembly (*33*, *34*). (iii) The third module is the assistant anti-inflammatory module composed of epigallocatechin gallate (EGCG) with antioxidant activity and inhibition of inflammatory cell activation to overcome the limited anti-inflammatory capacity of a single antioxidant (*25*).

Those three functional modules were assembled on the basis of the reported sandwiched layer-by-layer (LBL) self-assembly modification (*7*, *35*). EGCG with abundant phenolic hydroxyl groups was endowed between PEI-Tpl and nanogels to establish a sandwiched LBL coating and improve the overall performance of the multifunctional coating (*35*). In addition, EGCG also had protective effects on the endothelial cell function and inhibited SMC proliferation (*30*, *36*). HA, a typical component of glycocalyx, not only induces the adhesion and proliferation of endothelial cells but also promotes the conversion of SMCs to a contractile phenotype with low proliferation (*37*), instead of the synthetic phenotype, which causes restenosis at cardiovascular implantable devices. In this way, the self-regulating anticoagulant and self-defending anti-inflammatory coating mimicked the endothelial function and paved the way for the reendothelialization of cardiovascular implantable devices. The intrinsic pro-endothelial function of the coating, attributed to HA and EGCG, assists the endothelialization process. The coating showed aspirational prospects in improving the hemocompatibility and histocompatibility of cardiovascular implantable devices. The versatility of this strategy was demonstrated here by two representative models of biological valve leaflets and vascular stents.

RESULTS AND DISCUSSION

Preparation and in vitro RIVA release of thrombin-responsive nanogels

The Tpl-grafted PEI (PEI-Tpl) was synthesized by nitrophenyl chloroformate (NPC) reaction (fig. S1A) and characterized by ^{1}H nuclear magnetic resonance (NMR) spectra (fig. S1B). The fourier transform infrared spectrum (FI-IR) spectra of HA before and after oxidation are shown in fig. S2; the peak at about 1731 cm^{-1} (-C=O- stretching) indicated the successful oxidation of HA, which was consistent with other studies (*38*).

The nanogels were prepared by cross-linking between the amino group of cleavable peptide [NH_2-Gly-(D)CHA-Ala-Arg-Ser-Trp-Gly-$CONH_2$] and the aldehyde group of Ox-HA, named R@NG (fig. S3). The FI-IR spectra of nanogels (R@NG) and the mixture of Ox-HA, peptide, and RIVA (Ox-HA/peptide/RIVA) were detected (fig. S4). Compared to Ox-HA/peptide/RIVA, the new peak around 1644 cm^{-1} (C=N) that appeared in R@NG/EGCG/Tpl indicated the success of Schiff's base reaction. The particle size of the thrombin-triggered nanogels loaded with RIVA was about 189.90 ± 0.21 nm. The particle size of nanogels remained stable at the concentrations from 5 to 0.005 mg/ml, suggesting a covalent stable network of R@NG (fig. S5). The thrombin-sensitive performance of nanogels was investigated in phosphate-buffered saline (PBS) solution containing 5, 10, and 20 U/ml of thrombin. As shown in fig. S6, the particle size decreased with time and disordered particle size distribution was observed gradually under the stimulation of three different concentrations of thrombin, which indicated that thrombin triggers the disintegration of nanogels. In addition, the change of particle size was more violent with increasing thrombin concentration, suggesting the concentration-dependent response to thrombin.

We also investigated the RIVA release behavior of nanogels at different thrombin concentrations. As shown in Fig. 2A, both the amount and rate of RIVA release increased with the increasing thrombin concentration. The nanogels rapidly responded to the thrombin and then released most of the RIVA within 30 min, which ensured that the nanogels could release FXa-inhibiting anticoagulant RIVA immediately after contact with thrombin to block the coagulation. Furthermore, the low drug loss rate of the nanogels in the absence of thrombin stimulation (about 10%) allowed nanogels to preserve functional substances without external stimuli.

Preparation and characterization of the coating

The coating system, with thrombin-triggered self-regulating anticoagulant ability and anti-inflammatory capacity, was obtained by sequential assembly of PEI-Tpl, EGCG, and R@NG on the basis of sandwiched LBL self-assembly modification, named R@NG/EGCG/Tpl. The coating named R@NG/Tpl was obtained by sequentially dipping the substance into the solution of PEI-Tpl and R@NG.

The surface morphology of R@NG/Tpl and R@NG/EGCG/Tpl coatings was investigated by scanning electron microscopy (SEM) and atomic force microscopy (AFM). As shown in Fig. 2B, nanogels were observed on the surfaces of R@NG/Tpl and R@NG/EGCG/Tpl. The increased number of nanogels in R@NG/EGCG/Tpl compared with R@NG/Tpl indicated that the addition of EGCG improved the assembly of the nanogels on the coating. According to the AFM data (Fig. 2C), the surface roughness of R@NG/EGCG/Tpl was higher than that of R@NG/Tpl due to the increase of surface particles, which was consistent with the results of SEM. The presence of EGCG in R@NG/EGCG/Tpl was verified by ultraviolet-visible (UV-vis) spectrum (Fig. 2D). The adsorption band around 214 nm and the wide band between 270 and 290 nm in R@NG/EGCG/Tpl indicated the existence of natural EGCG and slightly oxidized EGCG (*35*). EGCG, rich in phenolic hydroxyl groups, worked as the weak cross-linker and imparted intermolecular forces to the coating, such as hydrogen bonds with nanogels and electrostatic interactions with PEI-Tpl. In addition, slightly oxidized EGCG with a small amount of *o*-quinones could form covalent bonds with primary amines in PEI-Tpl through Michael addition or Schiff base reaction (*7*, *35*).

The surface zeta potential shift of the coatings during the assembly process is shown in Fig. 2E. The final surface zeta potential at pH 7.4 of R@NG/Tpl was about +4.38 mV, while the zeta potential of R@NG/EGCG/Tpl (+3.25 mV) was slightly lower due to the negatively charged EGCG. The real-time assembly process of R@NG/Tpl and R@NG/EGCG/Tpl was investigated by quartz crystal microbalance with dissipation (QCM-D). The frequency shift (ΔF) indicated the adsorbed mass, and the dissipation variation (ΔD) indicated the soft state of the adsorbates. The high and low $\Delta D/\Delta F$ represented the

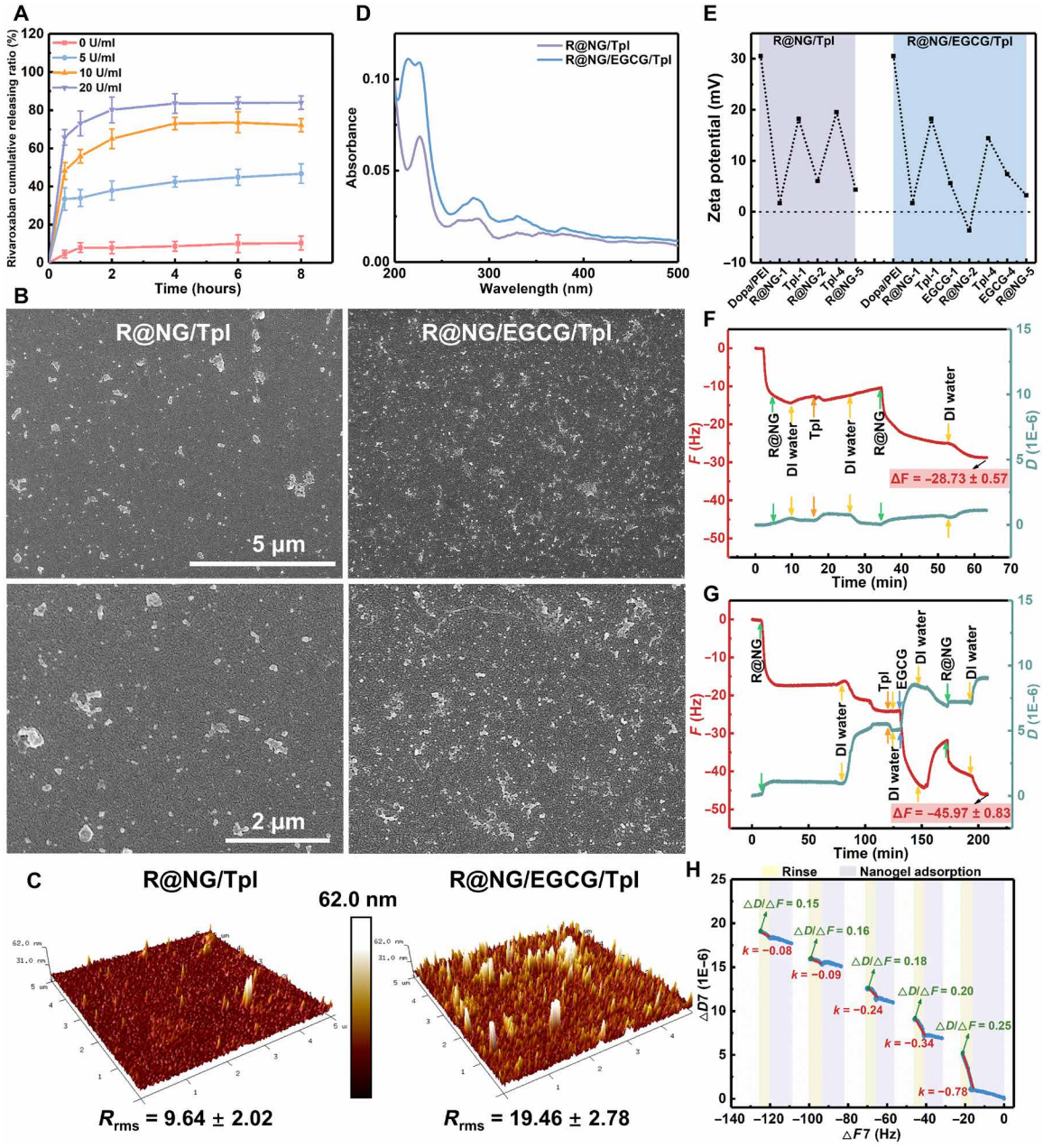

Fig. 2. Characterization of nanogels and coating. (**A**) Accumulated RIVA release from thrombin-sensitive nanogels in PBS with different thrombin concentrations. (**B**) SEM and (**C**) AFM images of R@NG/Tpl and R@NG/EGCG/Tpl. (**D**) UV-vis spectra of R@NG/Tpl and R@NG/EGCG/Tpl on a quartz substrate. (**E**) Surface zeta potential of R@NG/Tpl and R@NG/EGCG/Tpl at pH 7.4. Real-time monitoring of (**F**) R@NG/Tpl and (**G**) R@NG/EGCG/Tpl assembly with QCM-D. (**H**) ΔD-ΔF curve of nanogel layers in R@NG/EGCG/Tpl coating.

soft and rigid state of the adsorbed layer, respectively. The typical frequency and dissipation variations of the coating were shown in Fig. 2 (F and G). The frequency variation of R@NG/EGCG/Tpl (45.97 ± 0.83 Hz) was increased compared with R@NG/Tpl (33.48 ± 0.57 Hz), which indicated the higher adsorption of the coating components. Unlike the other layers, the frequency of the nanogel layer continued to increase during the desorption process [deionized (DI) water], due to the water absorption of the nanogels. The $\Delta D/\Delta F$ value of all nanogel layers in R@NG/EGCG/Tpl coating (Fig. 2H) was obtained by analyzing the F-time and D-time curves (fig. S7). The difference between the $\Delta D/\Delta F$ values of the desorption and adsorption became smaller as the number of layers increased, and the $\Delta D/\Delta F$ values in the desorbed state gradually decreased, indicating that the nanogel layer became more rigid and its water absorption decreased. The rate of change in $\Delta D/\Delta F$ decreased with increasing number of layers, which suggested that the coating became more stable during the assembly process.

In vitro thrombin-sensitive RIVA release and stability of coating

The thrombin-triggered self-regulating anticoagulant function was based on the thrombin-triggered RIVA release behavior of the

coating. R@NG/EGCG/Tpl was alternately immersed every 2 hours for two cycles in solutions with and without thrombin. As shown in Fig. 3A and fig. S8, the pulsatile release curve of RIVA suggested a rapid response to thrombin and the repeatable release of RIVA. Furthermore, to investigate the stability of R@NG/EGCG/Tpl without thrombin stimulation, we quantified the RIVA release from R@NG/EGCG/Tpl after 28 days of exposure to PBS. After 28-day immersion, about 65.3% of the initially loaded amount remained in the nanogels (Fig. 3B). In addition, we observed the morphology of R@NG/EGCG/Tpl after immersion in PBS for 7 days (R@NG/EGCG/Tpl-7) and 14 days (R@NG/EGCG/Tpl-14) (Fig. 3, C and D). A large number of nanogels were still present on the surface of R@NG/EGCG/Tpl-7, which was not much different from R@NG/EGCG/Tpl. Some of the nanogels were shed on the surface of R@NG/EGCG/Tpl-14, but a high number of nanogels remained to be observed. In summary, R@NG/EGCG/Tpl was capable of self-regulation by releasing anticoagulant drugs on demand due to the sensitivity to thrombin and reduced undesired drug loss to limit the coagulation risk in vitro.

In vitro anti-inflammatory assay

Inflammatory response can occur quite vigorously after implantation of a blood-contacting material. Monocytes in the blood arriving

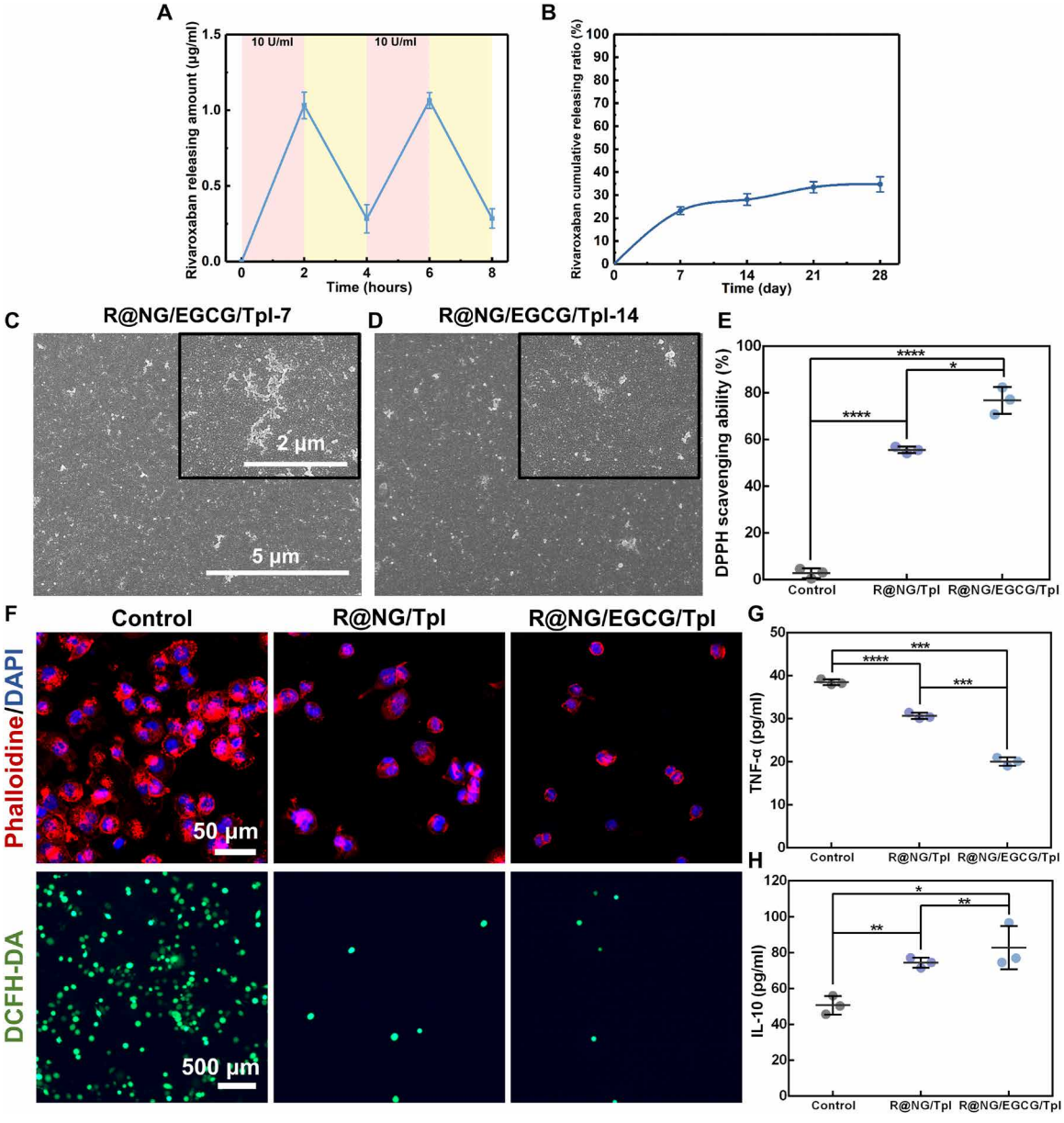

Fig. 3. Stability and anti-inflammatory capacity of the coating. (**A**) Pulsatile release profile of RIVA from R@NG/EGCG/Tpl under phasic exposure to the thrombin concentration of 10 U/ml. (**B**) RIVA loss rate of R@NG/EGCG/Tpl immersed in PBS at 37°C over 28 days. SEM images of R@NG/EGCG/Tpl after being immersed in PBS at 37°C for 7 days (**C**) and 14 days (**D**). (**E**) DPPH radical scavenging capability of the coatings. Fluorescence images of the (**F**) morphology and ROS generation of 160 nM PMA-treated THP-1 cells on different samples after 48 hours. Scale bar, 50 μm. (**G**) TNF-α and (**H**) IL-10 levels expressed by THP-1 cells detected by ELISA. $^{*}P < 0.05$, $^{**}P < 0.01$, $^{***}P < 0.001$, and $^{****}P < 0.0001$ (*t* test, error bars are defined as SD).

at the implantation site undergo phenotypic changes and differentiate into macrophages (*6*). A high level of proinflammatory free radicals, secreted by macrophages, enhances the inflammatory response and cell damage (*24*). In addition, the invasion of inflammatory cells induces coagulation, endothelialization disorder, and excessive proliferation of SMCs (*39*, *40*).

The free radical scavenging capacity of the coatings was investigated by 2,2-diphenyl-1-picrylhydrazyl (DPPH) assay (*7*), and the result was shown in Fig. 3E. In terms of absorbance values, both R@NG/Tpl and R@NG/EGCG/Tpl showed the potent ability to scavenge free radicals, but in comparison, the DPPH elimination rate of R@NG/EGCG/Tpl was approximately 38.13% higher than that of R@NG/Tpl. The free radical scavenging capacity of the coating apparently was mainly contributed by Tpl (*25*, *31*, *34*) and further enhanced by the endowed antioxidant EGCG (*37*). In addition to acting as a weak cross-linking agent, the antioxidant EGCG also helped to improve the anti–free radical properties of the coating.

To investigate the response of monocytes to the coatings, we incubated the samples with induced human monocytic leukemia cell line (THP-1 cells). As shown in Fig. 3F, the largest number of macrophages in activated states was observed on the surface of the control group. Compared with that, the number and activation degree of macrophages on the surfaces of both R@NG/Tpl and R@NG/EGCG/Tpl were substantially lower. The intracellular ROS production in macrophages was probed by 2′,7′-dichlorodihydrofluorescein diacetate (DCFH-DA), and as shown in Fig. 3F, macrophages in the control group displayed a higher level of ROS, while the fluorescent signals of R@NG/Tpl and R@NG/EGCG/Tpl were substantially attenuated. Furthermore, in R@NG/Tpl and R@NG/EGCG/Tpl groups, the expression levels of proinflammatory cytokine tumor necrosis factor–α (TNF-α) decreased and immunosuppressive cytokine interleukin-10 (IL-10) increased compared with the control group (Fig. 3, G and H). TNF-α is mainly secreted by classically activated macrophages, while IL-10 is released by regulatory macrophages to dampen immune responses (*41*, *42*). In addition to the antioxidant Tpl, HA also contributed to the anti-inflammatory properties of R@NG/Tpl, which exhibited anti-inflammatory activity and inhibited the release of monocyte cytokines. Combined with the results of the DPPH assay, it can be concluded that, in all experimental results, R@NG/EGCG/Tpl performed the best anti-inflammatory activity among the three groups due to the antioxidant and anti-inflammatory EGCG. As an anti-inflammatory agent, EGCG was proven to inhibit the TNF-α expression and up-regulate the IL-10 expression, thereby suppressing the activation of inflammatory cells (*36*). On the basis of the above, it was substantiated that the R@NG/EGCG/Tpl coating inhibited the inflammation of macrophages differentiated from monocytes by suppressing free radical production and regulating the expression of inflammation-related proteins.

From the above results, it is concluded that the addition of EGCG improved the assembly and free radical elimination capacity of the coating, resulting in a greater anticoagulant and anti-inflammatory potential of R@NG/EGCG/Tpl compared to R@NG/Tpl. Therefore, the subsequent characterization focused on R@NG/EGCG/Tpl.

In vitro platelet adhesion assay

Biomaterial incubation with platelet-rich plasma to observe platelet adhesion and activation on the surface of the material is a common method to analyze the antithrombotic properties (*43*, *44*). To further investigate the antithrombotic activity, platelet adhesion on the samples was inspected by SEM, and the results are shown in Fig. 4A. A large number of activated spread platelets with pseudopods were on the surface of control, while only a few low-activated discoid platelets were observed on the surface of R@NG/EGCG/Tpl. We also categorized and quantified the morphological differences between the two groups, according to the degree of activation (*45*). As shown in fig. S9, 40.97% of the platelets in the control group belonged to class 3, while only 23.16% belonged to class 3 in R@NG/EGCG/Tpl. The percentage of inactivated platelets (class 1) was 0% in the control group, while in R@NG/EGCG it was 11.36%. Notably, the quantitative results of platelet adhesion (Fig. 4B) also confirmed that the number of adherent platelets in the control group was much higher than that in the R@NG/EGCG/Tpl group. To sum up, R@NG/EGCG/Tpl performed excellent anti-platelet activation function and showed the potential to improve the hemocompatibility of blood-contacting biomaterials. The anticoagulant ability of the coating was further validated in different specific material models.

Cell morphology and proliferation of HUVECs and HUASMCs

Rapid endothelialization and early inhibition of smooth muscle hyperproliferation are common requirements for most cardiovascular implants (*12*), which are key to ideal material-host integration and avoidance of late thrombosis, late restenosis, and material failure. Considering the favorable antithrombotic and anti-inflammatory capacity, R@NG/EGCG/Tpl was selected for the subsequent experiments.

The proliferation of primary human umbilical vein endothelial cells (HUVECs) was investigated by fluorescent microscopy and the metabolic cell counting kit-8 (CCK-8) assay. As shown in Fig. 4C, the cell adhesion and proliferation number of HUVECs on the surface of R@NG/EGCG/Tpl were significantly higher than those of the control group, consistent with the results of the CCK-8 assay (Fig. 4D). In addition, most of the cells on the surface of R@NG/EGCG/Tpl showed a healthy spindle-shaped morphology. In contrast, the cell morphology of primary human umbilical artery SMCs (HUASMCs) on the surface of R@NG/EGCG/Tpl was substantially smaller and rounder than that of the control group (Fig. 4E). The CCK-8 assay (Fig. 4F) also showed that the proliferation on the surface of R@NG/EGCG/Tpl was inhibited. The size of HUASMCs was further analyzed by calculating the mean area of individual cells (fig. S10), and the results were consistent with the conclusion above. In addition, we quantified cell morphology by analyzing the mean value of the radius ratio, the ratio of the maximum concentric radius to the minimum concentric radius of the cell. As shown in Fig. 4G, the mean radius ratio of R@NG/EGCG/Tpl was significantly lower than that of the control group after both 24 and 72 hours, which suggested that the cell morphology of HUASMCs on the surface of R@NG/EGCG/Tpl was rounder than that of the control group. EGCG generally protects endothelial cell function and inhibits SMC proliferation (*30*, *36*). HA had been demonstrated to induce the adhesion and proliferation of endothelial cells by binding to CD44 and the receptor for HA-mediated motility (*46*). In addition, HA also promotes the conversion of SMCs to a contractile phenotype with low proliferation (*37*), which might contribute to the observed decreased proliferation rate of SMCs in R@NG/EGCG/Tpl with cross-linked HA. The different effects of R@NG/EGCG/Tpl coating on HUVECs and HUASMCs suggested that the coating had the potential to reduce cardiovascular material failure caused by delayed endothelialization and smooth muscle hyperproliferation.

In summary, the R@NG/EGCG/Tpl coating with self-regulating anticoagulant strategy and anti-inflammatory capacity exhibited potential self-regulating anticoagulation and effective elimination

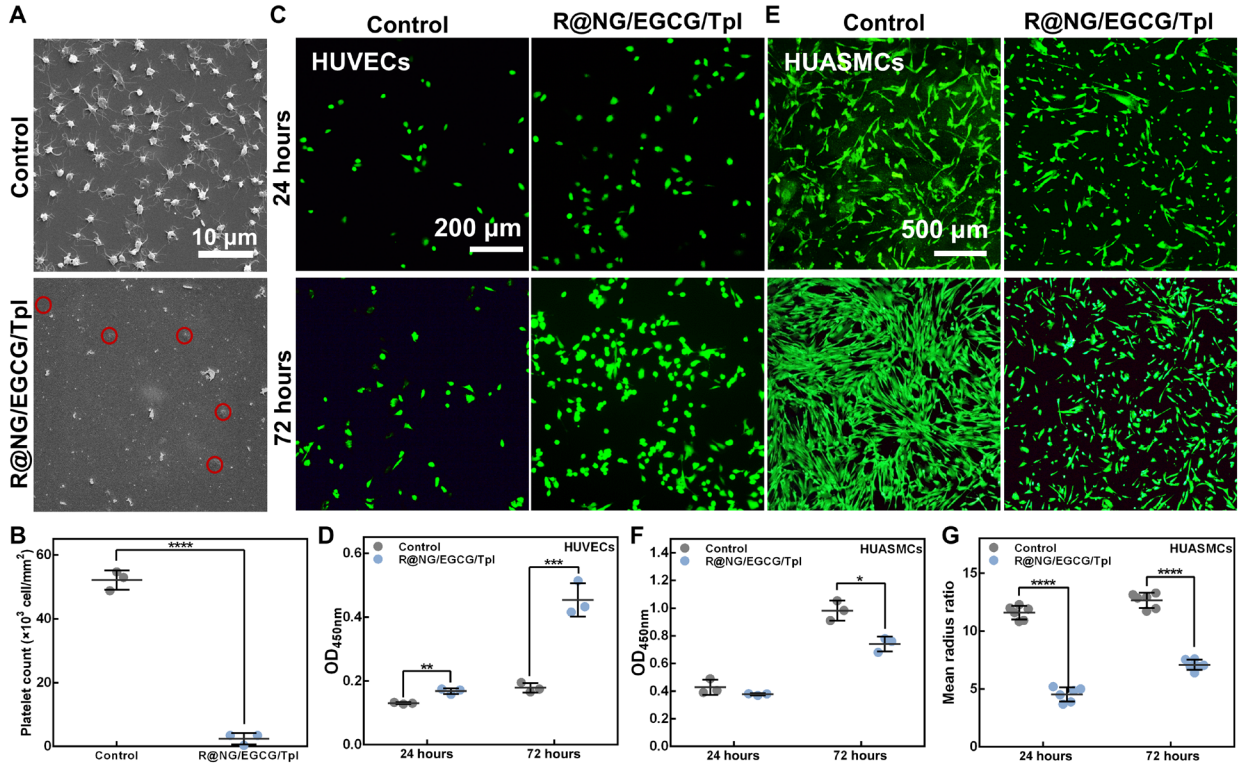

Fig. 4. Anticoagulation and cytotoxicity. (**A**) Platelet adhesion and activation on the surface of samples. (**B**) Number of platelets adhering to the surface of samples. (**C**) Fluorescence images of HUVECs stained by calcein and (**D**) cell viability of HUVECs cultured on the samples after 24 and 72 hours. Scale bar, 200 μm. (**E**) Fluorescence images of HUASMCs stained by calcein. Scale bar, 500 μm. (**F**) Cell viability and (**G**) mean radius ratio of HUASMCs on the samples after 24 and 72 hours. *$P < 0.05$, **$P < 0.01$, ***$P < 0.001$, and ****$P < 0.0001$ (*t* test, error bars are defined as SD).

of free radicals, paving the way for endothelialization. The intrinsic pro-endothelial function should further facilitate the rapid complete endothelialization of blood-contacting material, achieving the integration of the material in the host and maximizing the function of the cardiovascular devices. Hence, this coating apparently fulfills all requirements for surface modification of blood-contacting materials, as verified in the two specific applications below.

Modification on biological valve leaflets

Bioprosthetic heart valves are widely used in heart valve replacement, and most biological heart valves in the clinic are cross-linked with glutaraldehyde, which usually suffer from coagulation reaction, inflammation, and calcification (*47*, *48*). To investigate the potential improvement of GLUT biological valve leaflets, the R@NG/EGCG/Tpl coating was modified on GLUT.

The mechanical properties, thermal shrinkage temperature, and collagenase degradation of leaflets were investigated, and the results (Fig. 5, A to C) indicated that the R@NG/EGCG/Tpl coating did not significantly affect the mechanical property and collagen stability of the leaflets. The morphologies of GLUT cross-linked biological leaflets with and without modification were observed with SEM (Fig. 5D). After modification, the fibrous structure of the biological valve leaflets remained clear and was uniformly covered by the nanogel embedded coating.

The ex vivo arteriovenous shunt assay was conducted to investigate the antithrombotic property of the modified valve leaflets under real blood conditions, as indicated in the schematic diagram in Fig. 5E. We stuck the biological valve leaflets on the inner wall of polyvinyl chloride (PVC) tube tightly, which was connected with the carotid artery and jugular vein of the rabbit to form a circuit. The blood circulation continued for 1 hour, and the results were shown in Fig. 5 (F and G). After 1-hour blood circulation, severe thrombosis with cross-linked fibrin, activated platelets, and erythrocytes (Fig. 5F) was observed on the surface of GLUT. No thrombus was observed on R@NG/EGCG/Tpl, but only a small number of platelets with low activation levels. In addition, the thrombus weight on R@NG/EGCG/Tpl was significantly lower than that on GLUT (Fig. 5G). In conclusion, the self-regulating anticoagulant R@NG/EGCG/Tpl coating was suitable and effective for improving the anticoagulant properties of the biological valve leaflets.

Biological valve leaflets were implanted subcutaneously in male Sprague-Dawley rats to analyze the host response in vivo. Subcutaneous implantation is a common model for investigating the direct effects of the biomaterials at the implant site. The thickness of the fibrous capsule surrounding the implant indicates the histocompatibility of the material and the inflammatory response of the organism (*49*). After 15-day implantation, according to the hematoxylin and eosin (H&E) staining results (Fig. 5, H and I), the R@NG/EGCG/Tpl group presented milder inflammatory cell infiltration and thinner fibrous capsules compared to the GLUT group. After 30 days, the inflammatory response was still intense in the GLUT group, while it was reduced in the R@NG/EGCG/Tpl group. Furthermore, the TNF-α expression level was higher in the GLUT group than in the R@NG/EGCG/Tpl group on both days 15 and 30, while the IL-10 expression

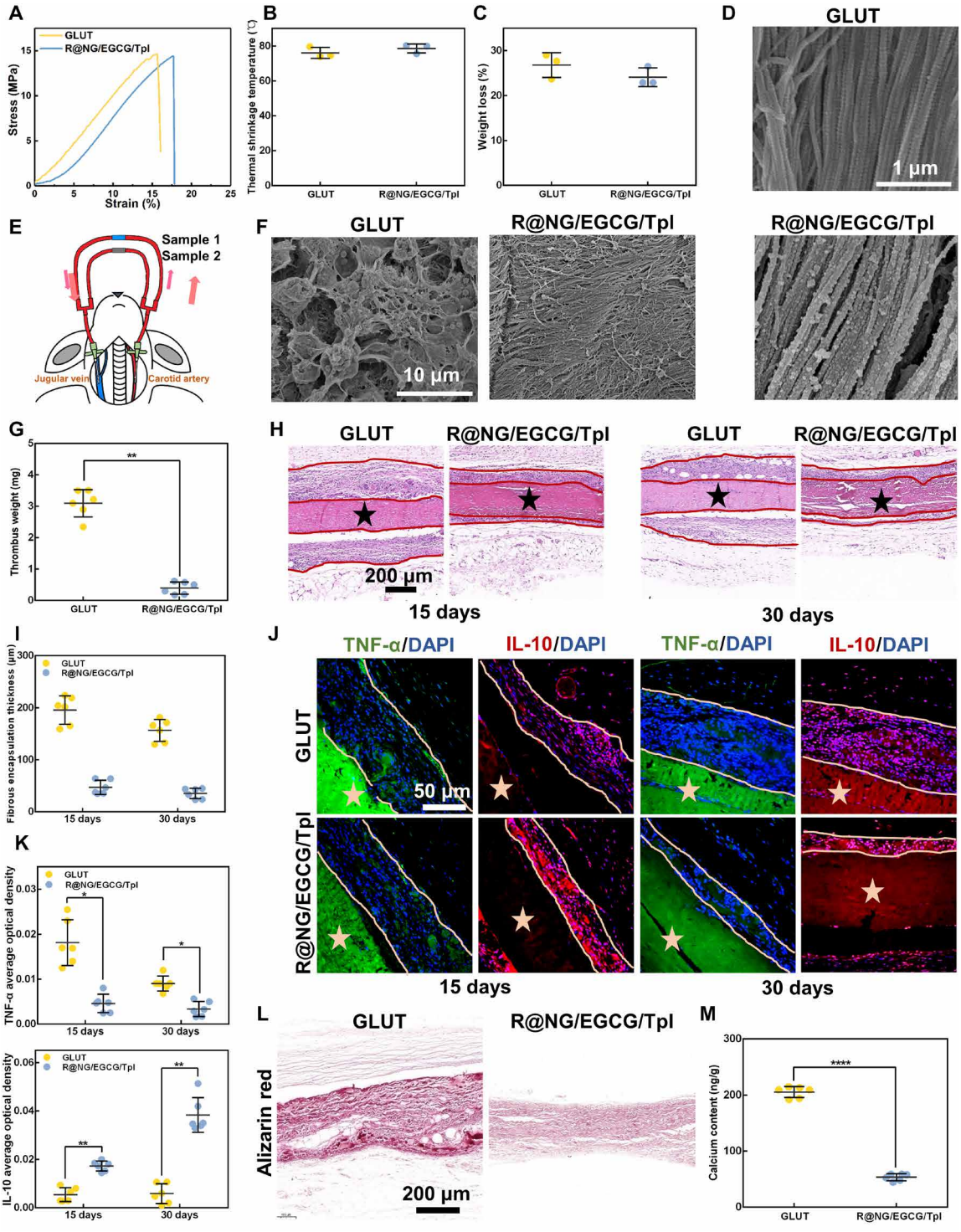

Fig. 5. Performance of the coating on biological valve leaflets. (**A**) Representative stress-strain curves, (**B**) thermal shrinkage temperature, and (**C**) weight loss ratio of biological valve leaflets. (**D**) Morphology of biological valves with and without R@NG/EGCG/Tpl modification observed by SEM. Scale bar, 1 μm. (**E**) Schematic diagram of the ex vivo arteriovenous shunt model. (**F**) SEM images and (**G**) thrombus weight of biological valve leaflets after 1-hour ex vivo arteriovenous shunt assay. Scale bar, 10 μm. (**H**) Photographs and (**I**) quantitative analysis of H&E staining of biological valve leaflets subcutaneously implanted in Sprague-Dawley rats. Scale bar, 200 μm. (**J**) Photographs of immunofluorescence analysis of biological valve leaflets. Scale bar, 50 μm. Capsules were traced by lines, and biological valves were marked by stars. (**K**) Quantitative data of immunofluorescence analysis of the capsule surrounding biological valve leaflets. Calcium deposits on biological valve leaflets characterized by (**L**) alizarin red staining and (**M**) ICP-OES. Scale bar, 200 μm. *$P < 0.05$, **$P < 0.01$, and ****$P < 0.0001$ (*t* test, error bars are defined as SD).

level of GLUT was lower than that in the R@NG/EGCG/Tpl group (Fig. 5, J and K). Thus, R@NG/EGCG/Tpl, with the ability to scavenge free radicals and inhibit the inflammatory response of macrophages, substantially reduced the in vivo inflammatory response of the GLUT cross-linked biological valve leaflets.

For GLUT cross-linked biological valves, one of the main causes of dysfunction is calcification, which can be induced by several factors, mainly residual cytotoxic aldehyde groups and free carboxyl groups that easily bond with calcium ions. In addition, calcification can be further aggravated by coagulation and inflammation. (*50*, *51*). The calcification after subcutaneous implantation was determined by alizarin red staining and inductively coupled plasma optical emission spectrometry (ICP-OES) (*52*, *53*). After 60 days of implantation, numerous red calcified spots were observed in the GLUT cross-linked valve tissue (Fig. 5L), while no notable calcified spots existed in R@NG/EGCG/Tpl. The quantitative analysis of calcium content by ICP-OES (Fig. 5M) further demonstrated the capacity of R@NG/EGCG/Tpl to prevent calcification. Since the calcification of glutaraldehyde cross-linked biological valve leaflets was mainly associated with the residual cytotoxic aldehyde groups, coagulation, and inflammation, the R@NG/EGCG/Tpl coating uniformly covering the surface of the original leaflet fibers shielded the residual aldehyde groups and thus reduced the calcification extent. In addition, the high cytocompatibility, histocompatibility, and anti-inflammatory properties of the coating also contributed to the protection from calcification. In summary, R@NG/EGCG/Tpl, with antithrombotic and anti-inflammatory abilities, could be a potential candidate for improving the performance of GLUT cross-linked biological valve leaflets.

Modification of vascular stents

Several factors contribute to the failure for vascular stents; chief among them are late stent thrombosis and late stent restenosis. As a typical blood-contacting cardiovascular implant, the vascular stent is expected to exhibit antithrombotic and anti-inflammatory properties, promote endothelialization, and inhibit SMC dysplasia. Poly (L-lactic acid) (PLA) stent is a promising class of absorbable vascular stents, and investigating new functional coated vascular stents or drug-eluting vascular stents to improve the performance of PLA vascular stents more comprehensively is one of the current directions (*54*). Here, we assembled the R@NG/EGCG/Tpl coating on the PLA vascular stents and investigated PLA sheets to investigate the potential of the multifunctional coating to improve the properties of vascular stents.

The morphologies of PLA vascular stents modified with the R@NG/EGCG/Tpl coating are shown in Fig. 6A, presenting multiple nanoparticles. The adhesion and flexibility of the coating on a stent are considered important as the stent undergoes crimping and expansion before implantation. The morphology of the modified stent dilated by an angioplasty balloon was analyzed. As shown in Fig. 6B, the R@NG/EGCG/Tpl coating remained intact without cracks and maintained the payload of nanogels after expansion. EGCG with abundant phenolic hydroxyl groups enhanced the interaction forces and the stability of the coating. In addition, the coating was assembled with hydrophilic PEI-Tpl, EGCG, and Ox-HA nanogels, where both PEI-Tpl and nanogels were of high molecular weight. Stent expansion was performed in a moist environment as the stent needed to be soaked in saline before implantation. Hydrophilic macromolecular interpenetrated substrate coatings and nanogels could swell under wet conditions, which also contributed to the resistance of deformation and avoidance of cracking. Those results indicated that the coating withstands the deformation and the nanogels would not be dislodged by deformation.

The ex vivo arteriovenous shunt assay was conducted to evaluate the antithrombogenic ability of R@NG/EGCG/Tpl-coated PLA vascular stents, and the results are shown in Fig. 6 (C and D). The hemocompatibility of the stents with the R@NG/EGCG/Tpl coating was significantly improved compared to bare PLA, and no severe thrombus was observed, suggesting that the self-regulating anticoagulant R@NG/EGCG/Tpl had an inhibitory effect on thrombosis and showed potential for application in improving the hemocompatibility of PLA vascular stents.

The host response of vascular stents modified with R@NG/EGCG/Tpl was detected by subcutaneous implantation of PLA sheets. As shown in Fig. 6 (E and F), the fibrous capsule on R@NG/EGCG/Tpl was much thinner than on the bare PLA sheet after 15 and 30 days. We further investigated the expression of inflammation-related factors TNF-α and IL-10 by immunofluorescence. Compared with PLA, the proinflammatory TNF-α expression levels were reduced on R@NG/EGCG/Tpl and anti-inflammatory IL-10 expression levels were increased after 15 and 30 days (Fig. 6, G and H). Collectively, the R@NG/EGCG/Tpl coating with anti-inflammatory PEI-Tpl and EGCG substantially suppressed the host response of PLA and showed potential to improve the histocompatibility of PLA vascular stents.

For further evaluation, the stents were implanted into the abdominal aorta of rabbits and explanted after 1 and 3 months. The cell morphology of the neointima on the inner surface was observed by SEM, and the brighter areas were the boundaries of the cells in the high-magnification SEM image, as shown in Fig. 7A. After 1 month, the boundaries on the surface of PLA were disordered, which meant that the cells covered on the bare PLA stents were not oriented. However, R@NG/EGCG/Tpl was fully covered by endothelial cells oriented in the direction of the blood flow. After 3 months, the cell layers in both two groups became denser, but still most of the boundaries remained random on the surface of PLA, suggesting that no obvious orientation was observed on the cells of the bare PLA group. For R@NG/EGCG/Tpl, almost all boundaries were horizontal, which oriented in the direction of the blood flow.

To assess the extent of endothelialization in more detail, we quantitatively analyzed immunofluorescent microphotographs (Fig. 7B). The cell number was reflected by cell nucleus area ratio, and the results (Fig. 7C) were consistent with SEM images. The number and orientation of cells on R@NG/EGCG/Tpl were substantially increased compared to the bare PLA vascular stents. CD31 is present at the tight junctions between endothelial cells, and high CD31 expression usually indicates an intact and healthy endothelial layer (*55*, *56*). The CD31 expression in the cell layers evaluated by immunofluorescence staining is shown in Fig. 7 (B and D). After 1 month of implantation, the CD31 expression was significantly higher on R@NG/EGCG/Tpl than on bare PLA. After 3 months, the cell density and CD31 expression of PLA stents were higher. However, CD31-positive cells in oval shape did not completely cover the stents. For the R@NG/EGCG/Tpl group, the CD31 expression was increased and CD31-positive cells were more closely aligned.

Endothelial NO synthase (eNOS) is an enzyme in healthy endothelial cells, which is involved in NO production (*49*). The eNOS expression in the neointima was investigated (Fig. 7, B and E) and showed consistent trends with the CD31 expression. Several factors were at play in the favorable pro-endothelialization function of

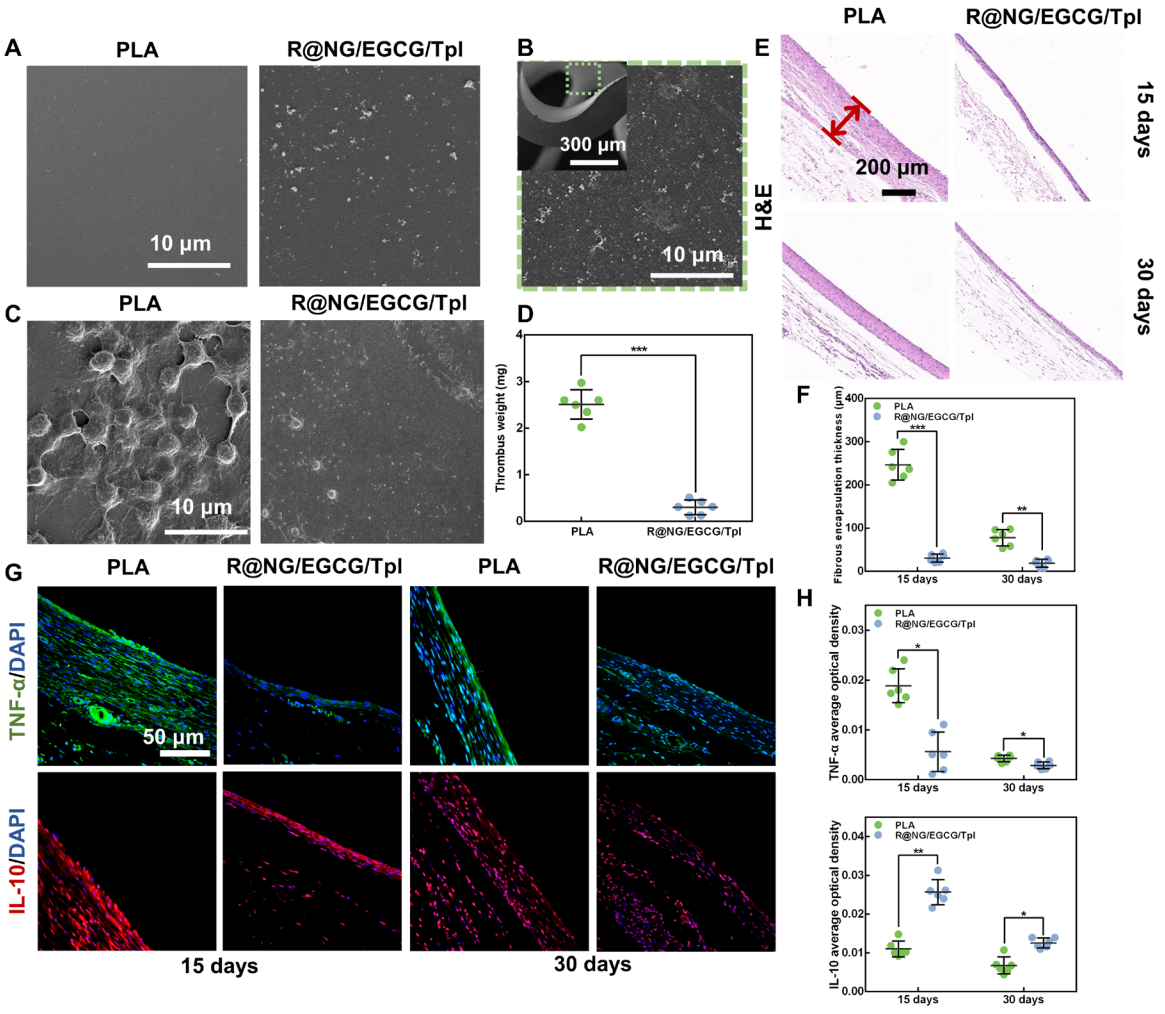

Fig. 6. Characterization, hemocompatibility, anticoagulation, and endothelialization of vascular stents modified with the coating. (**A**) SEM images of PLA vascular stents before and after R@NG/EGCG/Tpl modification. Scale bar, 10 μm. (**B**) SEM images of R@NG/EGCG/Tpl-modified vascular stent after dilation. Scale bars, 300 and 10 μm. (**C**) SEM images and (**D**) thrombus weight of vascular stents after blood circulation in ex vivo arteriovenous shunt assay for 1 hour. Scale bar, 10 μm. (**E**) Photographs and (**F**) quantitative analysis of histomorphological evaluation of subcutaneously implanted vascular stents. Scale bar, 200 μm. The fibrous encapsulation was marked by the red lines. (**G**) Photographs and (**H**) quantitative data of immunofluorescence analysis of subcutaneously implanted vascular stents. Scale bar, 50 μm. $^{*}P < 0.05$, $^{**}P < 0.01$, and $^{***}P < 0.001$ (*t* test, error bars are defined as SD).

R@NG/EGCG/Tpl. Foremost, the thrombin-triggered closed-loop anticoagulant coating counteracted the negative effects of thrombosis on endothelialization. In addition, the antioxidant capacity of the coating protected the endothelium from oxidative stress damage and facilitated endothelial proliferation.

The neointimal stenosis, inflammation, endothelialization, and hyperplasia of the stent cross sections were identified by H&E and immunohistochemical staining (Fig. 7F and fig. S11). The mean neointimal stenosis (Fig. 7G) of R@NG/EGCG/Tpl (22.30 ± 3.41%) was lower than that of bare PLA stents (37.17 ± 2.22%) after 1 month. The difference in neointimal stenosis was even more pronounced after the third month. The stenosis of bare PLA stents was as high as 76.94 ± 4.74%, while the stenosis rate was significantly lower in R@NG/EGCG/Tpl (26.98 ± 1.91%). From the above results, R@NG/EGCG/Tpl remarkably reduced restenosis in vivo.

Inflammation after stent implantation is especially harmful, as it causes or exacerbates restenosis and hyperproliferation of intima. According to the CD68 expression results (Fig. 7, F and H), the inflammatory response of the stents was remarkably suppressed after R@NG/EGCG/Tpl modification during the implantation period (*57*), which can be attributed to the excellent antioxidant and anti-inflammatory activity of the coating. Furthermore, the extremely low CD68 expression level at the third month also suggested the ideal histocompatibility and host integration of R@NG/EGCG/Tpl.

In addition to inflammation, restenosis is also related to the phenotype of SMCs. Contractile SMCs with low proliferation and migration play a vital role in maintaining the elasticity and contraction of blood vessels, which is the basis for the inhibition of SMC proliferation (*58*). As an indicator of contractile SMCs, α–smooth muscle actin (α-SMA) expression level was evaluated by immunohistochemical staining (Fig. 7, F and I). The α-SMA expression level of R@NG/EGCG/Tpl was significantly higher than that of bare stents. In addition, the α-SMA expression on PLA stents decreased over time, while it increased on R@NG/EGCG/Tpl. The R@NG/EGCG/Tpl coating promoted the

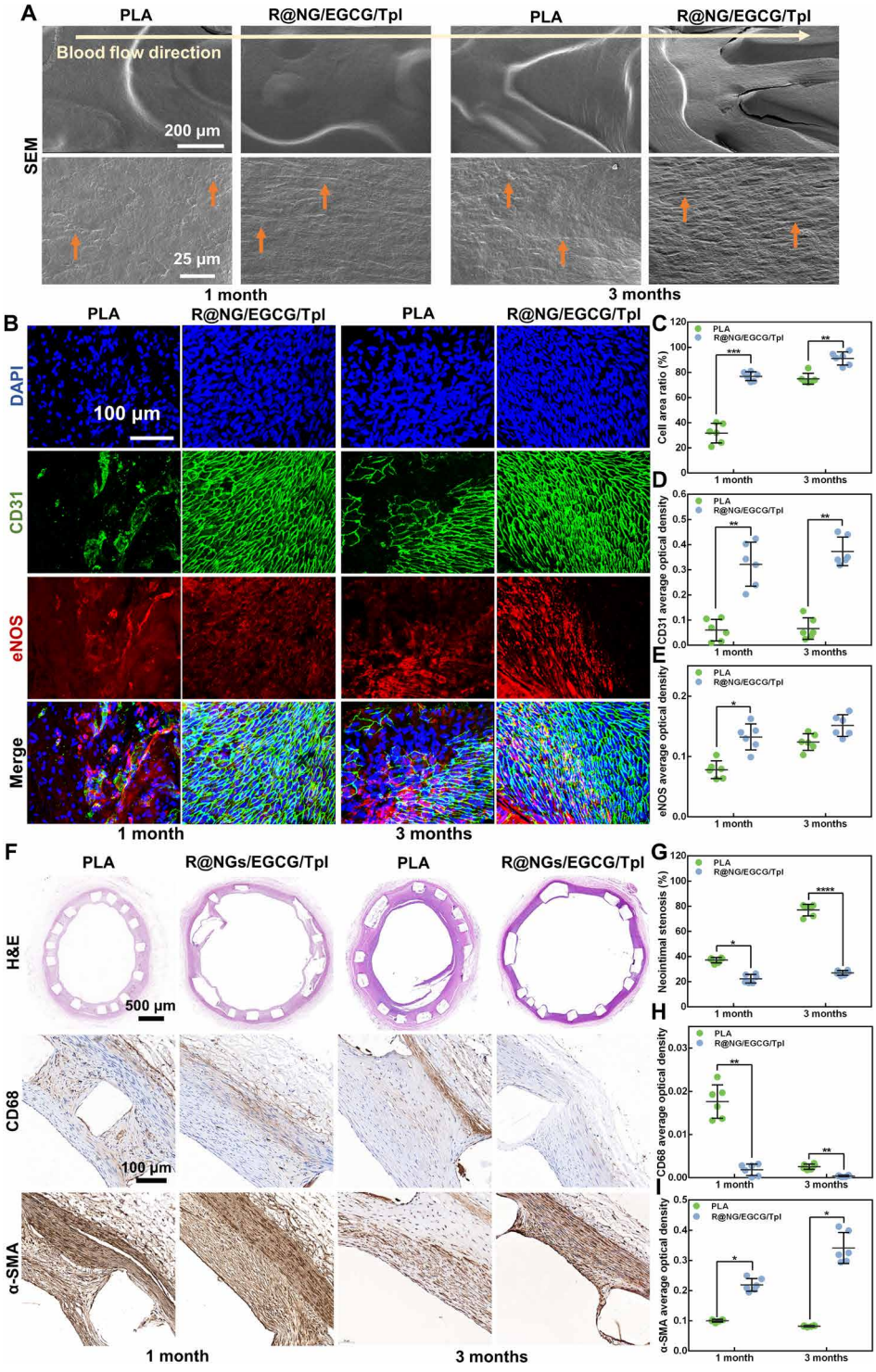

Fig. 7. In vivo histocompatibility of the vascular stent modified with the coating. (**A**) Morphology of the luminal vascular stents after implantation in the abdominal aorta of New Zealand rabbits observed by SEM. Scale bars, 200 and 25 μm. The representative cells oriented in the direction of the blood flow were marked with orange arrows. (**B**) Immunofluorescence analysis of the vascular stents after implantation in the abdominal aorta of New Zealand rabbits. Scale bar, 100 μm. Quantitative analysis of (**C**) cell area ratio, (**D**) CD31 expression, and (**E**) endothelial nitric oxide synthase (eNOS) expression of the vascular stents. (**F**) Histological and immunohistochemical analysis of the vascular stents after implantation in the abdominal aorta of New Zealand rabbits. Scale bars, 500 and 100 μm. Quantitative analysis of (**G**) neointimal stenosis, (**H**) CD68 expression, and (**I**) α-SMA expression of the abdominal aorta implanted with vascular stents. *$P < 0.05$, **$P < 0.01$, ***$P < 0.001$, and ****$P < 0.0001$ (*t* test, error bars are defined as SD).

conversion of SMCs to a contractile phenotype, which can be attributed to its HA and EGCG components. EGCG is able to inhibit the excessive proliferation of SMCs (*59*). Meanwhile, HA induces the migration of SMCs via CD44-mediated signaling and promotes the conversion of SMCs to a contractile phenotype (*38*).

In conclusion, the R@NG/EGCG/Tpl coating promoted endothelialization, decreased the inflammatory response, and increased the SMC contractile phenotype, thereby reducing restenosis and facilitating long-term stent patency. Hence, R@NG/EGCG/Tpl presents a potential and efficient vascular stent coating.

In summary, a thrombin-triggered self-regulating anticoagulant coating strategy with anti-inflammatory capacity was designed and synthesized by combining thrombin-sensitive nanogels loaded with the FXa inhibitor RIVA, antioxidant Tpl, and EGCG. In vitro drug release assay confirmed the feedback-controlled release of anticoagulant RIVA, and the excellent antithrombotic ability of R@NG/EGCG/Tpl was demonstrated by in vitro and ex vivo hemocompatibility evaluations. R@NG/EGCG/Tpl inhibited the activation of macrophages by eliminating free radicals and regulating the expression of inflammation-related proteins, which was attributed to the antioxidant Tpl and EGCG. Meanwhile, R@NG/EGCG/Tpl promoted the growth of endothelial cells and inhibited the excessive proliferation of SMCs.

The versatility of R@NG/EGCG/Tpl was demonstrated in two models of cardiovascular blood-contacting materials. The anticoagulant ability, tissue compatibility, and anticalcification capacity were enhanced in the modified biological valves. The vascular stents modified with R@NG/EGCG/Tpl exhibited improved hemocompatibility, host response, reendothelialization, and anti-hyperplastic activity, which were confirmed by in vitro and in vivo studies.

In this work, the physiological condition was complicated as it involved convective flow, unpredictable thrombin levels, viscous blood, and various blood protein. Simulating this complex and variable physiological conditions in vitro was a challenge and difficult to consider comprehensively. Therefore, thrombin sensitivity of R@NG was investigated by a simplified thrombin-stimulated environment (drug release and particle size variation of the nanogels and pulsatile drug release of R@NG/EGCG/Tpl). Although it is difficult to simulate the complex and changeable physiological environment in vitro, more investigations are needed in the future.

All in all, this thrombin-triggered self-regulating anticoagulant coating strategy with anti-inflammatory capacity inhibited various adverse consequences due to coagulation and inflammatory reactions, thus escorting the reendothelialization on the surface of cardiovascular implantable devices. This coating optimized the performance of cardiovascular blood-contacting materials and provided a new perspective for the design of endothelium-like functional coatings.

MATERIALS AND METHODS

Materials

Dopamine hydrochloride (Dopa), HA (M_w ~7000), branched PEI (average M_n ~10,000 by gel permeation chromatography), EGCG, phorbol 12-myristate 13-acetate (PMA), CCK-8, and Triton X-100 were purchased from Sigma-Aldrich (Shanghai, China). 4-Hydroxy-2,2,6,6-tetramethylpiperidine-1-oxyl (Tpl) and RIVA were purchased from Adamas Reagent Co. Ltd. (Shanghai, China). Heparin sodium salt (185 U/mg) was purchased from Shanghai Macklin Biochemical Co. Ltd. (Shanghai, China). The peptide NH_2-Gly-(D)CHA-Ala-Arg-Ser-Trp-Gly-$CONH_2$ was synthesized by GL Biochem Ltd. (Shanghai, China). Fresh porcine pericardium was provided by Venus MedTech Inc. (Hangzhou, China) and decellularized according to the previous report (*60*). The biodegradable poly (L-lactic acid) stents (PLA) were provided by Sichuan XingTai Pule Medical Equipment Co. Ltd. (Chengdu, China).

Synthesis of Ox-HA and PEI-Tpl

Sodium periodate ($NaIO_4$) solution (99.2 mg/ml) was added dropwise to a HA solution (25 mg/ml). After stirring for 24 hours in the dark, ethylene glycol (0.6 ml) was added to quench the reaction. Ox-HA was obtained by dialysis against DI water and freeze-drying.

Tpl (0.02 mol, 3.44 g) and triethylamine (0.03 mol, 4.35 ml) were dissolved in tetrahydrofuran (THF). p-NPC (0.022 mol, 4.44 g) in THF was added dropwise and stirred for 24 hours. Then, PEI (M_w = 25,000, 3.44 g) was dissolved in dimethyl sulfoxide (DMSO) and added into the reaction system. After stirring at room temperature for another 24 hours, PEI-Tpl was obtained by dialysis against DI water and freeze-drying. ^{1}H NMR spectra were used to characterize PEI-Tpl.

Coating preparation

Before modification, the substrates were pretreated with the classic mussel-mimicking amino-amplified coating obtained by copolymerization of dopamine and PEI, which could be prepared on a wide range of substrate materials. Considering the reliability of data collection, silicon wafers (Si), gold-plated quartz crystal, PLA, and biological valve leaflets were pretreated with the same coating and then modified with the anticoagulant coating system. Briefly, the substrates were immersed in dopamine solution (0.2 mg/ml in 10 mM tris buffer, pH 8.5) for 45 min. After that, PEI solution (40 mg/ml in 10 mM tris buffer, pH 8.5) of the same volume as the dopamine solution was added for another 30 min (named Dopa/PEI). The substrates were rinsed with DI water for further modification.

The substrates were immersed in nanogel solution for 12 hours (named R@NG). Then, they were sequentially immersed into the PEI-Tpl (2 mg/ml), EGCG (0.5 mg/ml), and R@NG solution. The coating cycle was repeated four times; the obtained coating is referred to as R@NG/EGCG/Tpl.

Silicon wafers were selected as substrates in the coating morphology section, in vitro thrombin-sensitive RIVA release and stability of coating section, in vitro anti-inflammatory assay section, in vitro platelet adhesion assay section, and cell morphology and proliferation of HUVEC and HUASMC section.

PLA mats were selected as substrates in the section of UV-vis spectrophotometer assay. Quartz plates were selected as substrates in the section of coating surface zeta potential.

Cell culture

The human monocytic leukemia cell line (THP-1, National Science & Technology Infrastructure) was cultured in RPMI 1640 medium containing 10% fetal bovine serum (FBS) and 1% penicillin/streptomycin at 37°C under a 5% CO_2 atmosphere. Primary HUVECs (West China Hospital in Sichuan University, China) and primary HUASMCs (West China Hospital in Sichuan University, China) were cultured in Dulbecco's modified Eagle's medium containing 10% FBS and 1% penicillin-streptomycin at 37°C in a 5% CO_2 atmosphere.

Preparation of thrombin-sensitive nanogels

Ox-HA (10 mg) and RIVA (2 mg) were dissolved in DMSO (5 ml), and then cleavable peptide solution (5 mg/ml, 2 ml) was slowly dropped

into the stirring solution at room temperature. After 7 hours, the mixed solution was dialyzed in DI water (molecular weight cut off = 1000) for another 12 hours at room temperature.

Characterization of the nanogels

The particle size of the nanogels was characterized by dynamic light scattering. The in vitro drug release behavior of the nanogels was investigated in different concentrations of thrombin solution (0, 5, 10, and 20 U/ml in PBS) at 37°C. Two milliliters of nanogel suspension (1 mg/ml) was added into a dialysis bag and incubated in thrombin solution under stirring. At predetermined time, 2 ml of the sample was taken out and 2 ml of fresh thrombin solution was added. The released RIVA was characterized by UV measurement.

Coating characterization

The micromorphology of the coating was observed by SEM (FEI Nova NanoSEM 450). The roughness of the coating was investigated by AFM (Bruker) using tapping mode with a ScanAsyst-Air (Triangular) cantilever.

The real-time construction process of the coating was monitored by QCM-D (QSense Analyzer, Biolin, Sweden), and data analysis was conducted with Dfind Smartfit modeling in QSense Dfind software. The coating was assembled on the 5-MHz gold-plated quartz crystal at a flow rate of 50 μl/min, and the concentration of the solution in QCM-D was consistent with the experimental concentration. Surface zeta potential changes during coating assembly were measured with a SurPASS 3 (Anton Paar, Austria) instrument. The existence of EGCG was determined with a UV-vis spectrophotometer (PerkinElmer LAMBDA 850, USA) in the range of 200 to 600 nm.

In vitro release of RIVA from the coating

R@NG/EGCG/Tpl (0.8 cm × 0.8 cm) was soaked into PBS containing thrombin (0 and 10 U/ml), periodically for 2 hours each. The amount of released RIVA was calculated using UV measurement.

R@NG/EGCG/Tpl (0.8 cm × 0.8 cm) was immersed in 3 ml of PBS at 37°C under shaking for 7, 14, 21, and 28 days. Every 2 days, 3 ml of PBS was withdrawn and 3 ml of fresh PBS was added. The released RIVA was determined by UV measurement. The coated sample was removed after 7 and 14 days of immersion, and surface morphology was investigated by SEM.

DPPH assay and in vitro anti-inflammation evaluation

The ability of the coatings for free radical elimination was investigated by DPPH assay. DPPH was dissolved in ethanol solution (95%, v/v) at 0.1 mM and incubated with the coatings at 37°C in the dark. After 30 min, the liquid was pipetted out and analyzed in a microplate reader (Synergy H1, BioTek Instruments Inc.) at 517 nm.

To evaluate the effect of the coating on monocytes, the substrates were placed into 24-well plates to coculture with monocytes. One milliliter of THP-1 cell suspension (5×10^4 cells) containing 160 nM PMA was seeded on the substrates. After 48-hour coculture, some adherent cells were fixed and stained with rhodamine-conjugated phalloidin and 4′,6-diamidino-2-phenylindole (DAPI) dyes and some with DCFH-DA (10 μM). The morphology and ROS generation of cells were observed with a confocal laser scanning microscope (CLSM) (Leica SP5, Germany). Enzyme-linked immunosorbent assay (ELISA) (Jingmei Biotechnology) was used to detect the TNF-α and IL-10 levels of the collected supernatants.

In vitro hemocompatibility evaluation

All animal experimental procedures were approved by the medical ethics committee of Sichuan Provincial Committee for Experimental Animal Management and performed in accordance with the guidelines for the care and use of laboratory animals of Sichuan University (no. KS2020394). Sprague-Dawley rats and New Zealand white rabbits used for studies were supplied by the West China Experimental Animal Center of Sichuan University (China). The coatings were incubated in 500 μl of rabbit platelet-rich plasma at 37°C. After 45 min, the coatings were taken out and rinsed three times with saline. Platelet adhesion and activation on samples were observed by SEM (FEI Nova NanoSEM 450).

Cell proliferation and morphology

One milliliter of HUVEC or HUASMC cell suspension containing around 2×10^4 cells was seeded on samples. After 1- and 3-day culture, the proliferation of cells on samples was characterized by a CCK-8 assay. The cells adherent to the samples were stained by calcein and observed with a fluorescence microscope.

Modification and characterization of biological valve leaflets

SEM was conducted to observe the micromorphology of biological valve leaflets before and after modification. The mechanical properties, thermal shrinkage temperature, and collagenase degradation tests were conducted to assess the effect of the coating on the mechanical properties and stability of the biological valve leaflets. The biological valve leaflets in a rectangular shape ($n = 4$) were subjected to mechanical property tests on the Instron 5967 Testing Machine (Instron, USA) at a constant velocity of 12.5 mm/min. The thermal shrinkage temperature of the biological valve leaflets was investigated with a DSC 2920 instrument (TA Instruments, Newcastle, DE) under a N_2 atmosphere. A collagenase degradation test was conducted on the biological leaflets. The dried biological leaflets were weighed (W_0) and then incubated with collagenase II (125 U/ml) in tris buffer (0.1 M tris, 50 mM $CaCl_2$, pH 7.4) at 37°C. After 24 hours, the biological valve leaflets were rinsed with DI water and weighed (W_t) after freeze-drying. The weight loss percentage was calculated by the following equation: $\Delta W\ \% = (W_0 - W_t)/W_0 \times 100$.

The ex vivo arteriovenous shunt assay was conducted according to the previous reports (*36*). In short, the biological valve leaflets were stuck on the inner wall of PVC tubes tightly, which were sterilized with ethyl alcohol and treated with heparin. After being anesthetized by pentobarbital, the left carotid artery and right jugular vein of male New Zealand white adult rabbits (weight, 2.5 to 3.0 kg) were isolated. The assembled tube was connected with the carotid artery and jugular vein to form a circuit. The blood circulation continued for 1 hour. Then, the test was terminated, and the leaflets were rinsed and fixed with paraformaldehyde. The clots on the surface of samples were collected and weighed. The samples were fixed and dehydrated before observation with SEM.

The dorsal skin of pentobarbital-anesthetized male juvenile Sprague-Dawley rats ($n = 6$, 3 weeks old, weighing 50 g) was surgically incised, and the biological valve leaflets were implanted into the subcutaneous pockets (two pockets on the back of each rat). The leaflets without neointima attached were explanted and fixed with paraformaldehyde after 60 days for the mineral analyses and histopathological examination. The amount of calcium was investigated by ICP-OES (VISTA-MPX, Varian Inc.), and the calcium deposition of leaflets was observed after alizarin red staining (*60*).

The inflammatory response was investigated by implanting the biological valve leaflets into male Sprague-Dawley rats (weighing 300 g) subcutaneously. After 15 and 30 days, the biological valve leaflets covered with the surrounding neointima were explanted and fixed with paraformaldehyde. The fixed tissues were stained with H&E for further investigation. The TNF-α and IL-10 expression was analyzed by immunofluorescence with DAPI counterstaining.

Modification and characterization of vascular stents

The surface of the vascular stent before and after dilatation with a 2.75-mm-diameter balloon under 8 atm pressure for 30 s was observed by SEM. The ex vivo arteriovenous shunt assay was conducted, and the experimental procedures were similar to that of the biological valve leaflets.

The PLA sheets modified with R@NG/EGCG/Tpl were implanted into male Sprague-Dawley rats (weighing 300 g) to investigate the inflammatory response after vascular stent implantation. After 15 and 30 days, the neointima around PLA sheet was explanted and fixed with paraformaldehyde. The experimental procedures and sample analysis were the same as for the subcutaneous biological valve leaflet implantation experiment.

The PLA vascular stents before and after modification were implanted into the abdominal aortic vessels of the healthy male New Zealand white adult rabbits ($n = 6$, weighing 2.5 to 3 kg) after anesthesia. After 1 and 3 months, the stents with surrounding vascular tissue were explanted and fixed with paraformaldehyde for 1 week. The inner wall of the stent was observed with SEM after dehydration. For immunofluorescent analysis, the inner wall of the tissue block was observed with CLSM after staining with anti-CD31, anti-eNOS, and DAPI. The neointimal stenosis of the vascular stent was calculated according to the H&E staining slices. The CD68 and α-SMA expression levels were investigated according to immunohistochemistry.

Statistical analysis

All experiments were repeated at least three times, and the results were expressed as means ± SD. One-way analysis of variance (ANOVA; *t* test) was used to determine statistical significances between different samples undergoing the same treatment. $^{*}P < 0.05$, $^{**}P < 0.01$, $^{***}P < 0.001$, and $^{****}P < 0.0001$. Histomorphometric, immunohistochemical, and immunofluorescent staining results were analyzed by Image-Pro Plus software.

SUPPLEMENTARY MATERIALS

Supplementary material for this article is available at https://science.org/doi/10.1126/sciadv.abm3378

REFERENCES AND NOTES

1. F. Bartoli-Leonard, E. Aikawa, Heart valve disease: Challenges and new opportunities. *Front. Cardiovasc. Med.* **7**, 602271 (2020).
2. E. S. Fioretta, S. E. Motta, V. Lintas, S. Loerakker, K. K. Parker, F. P. T. Baaijens, V. Falk, S. P. Hoerstrup, M. Y. Emmert, Next-generation tissue-engineered heart valves with repair, remodelling and regeneration capacity. *Nat. Rev. Cardiol.* **8**, 92–116 (2020).
3. G. Crimi, V. Gritti, V. A. Galiffa, V. Scotti, S. Leonardi, M. Ferrario, M. Ferlini, G. M. De Ferrari, L. Oltrona Visconti, C. Klersy, Drug eluting stents are superior to bare metal stents to reduce clinical outcome and stent-related complications in CKD patients, a systematic review, meta-analysis and network meta-analysis. *J. Interv. Cardiol.* **31**, 319–329 (2018).
4. E. S. Fioretta, S. E. Motta, V. Lintas, S. Loerakker, K. K. Parker, F. P. T. Baaijens, V. Falk, S. P. Hoerstrup, M. Y. Emmert, Next-generation tissue-engineered heart valves with repair, remodelling and regeneration capacity. *Nat. Rev. Cardiol.* **18**, 92–116 (2021).
5. D. Radke, W. Jia, D. Sharma, K. Fena, G. Wang, J. Goldman, F. Zhao, Tissue engineering at the blood-contacting surface: A review of challenges and strategies in vascular graft development. *Adv. Healthc. Mater.* **7**, 1701461 (2018).
6. S. Franz, S. Rammelt, D. Scharnweber, J. C. Simon, Immune responses to implants – a review of the implications for the design of immunomodulatory biomaterials. *Biomaterials* **32**, 6692–6709 (2011).
7. B. Zhang, R. Yao, C. Hu, M. Maitz, H. Wu, K. Liu, L. Yang, R. Luo, Y. Wang, Epigallocatechin gallate mediated sandwich-like coating for mimicking endothelium with sustained therapeutic nitric oxide generation and heparin release. *Biomaterials* **269**, 120418 (2021).
8. M. Gorbet, C. Sperling, M. F. Maitz, C. A. Siedlecki, C. Werner, M. V. Sefton, The blood compatibility challenge. Part 3: Material associated activation of blood cascades and cells. *Acta Biomater.* **94**, 25–32 (2019).
9. M. F. Maitz, M. C. L. Martins, N. Grabow, C. Matschegewski, N. Huang, E. L. Chaikof, M. A. Barbosa, C. Werner, C. Sperling, The blood compatibility challenge. Part 4: Surface modification for hemocompatible materials: Passive and active approaches to guide blood-material interactions. *Acta Biomater.* **94**, 33–43 (2019).
10. L. Bai, J. Zhao, Q. Li, J. Guo, X. Ren, S. Xia, W. Zhang, Y. Feng, Biofunctionalized electrospun PCL-PIBMD/SF vascular grafts with PEG and cell-adhesive peptides for endothelialization. *Macromol. Biosci.* **19**, e1800386 (2019).
11. J. Zhang, L. He, G. Wei, X. Jiang, L. Fu, Y. Zhao, L. Zhang, L. Yang, Y. Li, Y. Wang, H. Mo, J. Shen, Zwitterionic polymer-grafted polylactic acid vascular patches based on a decellularized scaffold for tissue engineering. *ACS Biomater Sci. Eng.* **5**, 4366–4375 (2019).
12. N. Lyu, Z. Du, H. Qiu, P. Gao, Q. Yao, K. Xiong, Q. Tu, X. Li, B. Chen, M. Wang, G. Pan, N. Huang, Z. Yang, Mimicking the nitric oxide-releasing and glycocalyx functions of endothelium on vascular stent surfaces. *Adv. Sci.* **7**, 2002330 (2020).
13. F. Zhang, Q. Zhang, X. Li, N. Huang, X. Zhao, Z. Yang, Mussel-inspired dopamine-CuII coatings for sustained in situ generation of nitric oxide for prevention of stent thrombosis and restenosis. *Biomaterials* **194**, 117–129 (2019).
14. G. M. Arepally, T. L. Ortel, Heparin-induced thrombocytopenia. *Annu. Rev. Med.* **61**, 77–90 (2010).
15. T. Xue, B. Peng, M. Xue, X. Zhong, C. Y. Chiu, S. Yang, Y. Q. Qu, L. Y. Ruan, S. Jiang, S. Dubin, R. B. Kaner, J. I. Zink, M. E. Meyerhoff, X. F. Duan, Y. Huang, Integration of molecular and enzymatic catalysts on graphene for biomimetic generation of antithrombotic species. *Nat. Commun.* **5**, 3200 (2014).
16. M. F. Maitz, J. Zitzmann, J. Hanke, C. Renneberg, M. V. Tsurkan, C. Sperling, U. Freudenberg, C. Werner, Adaptive release of heparin from anticoagulant hydrogels triggered by different blood coagulation factors. *Biomaterials* **135**, 53–61 (2017).
17. M. F. Maitz, U. Freudenberg, M. V. Tsurkan, M. Fischer, T. Beyrich, C. Werner, Bio-responsive polymer hydrogels homeostatically regulate blood coagulation. *Nat. Commun.* **4**, 2168 (2013).
18. J. Yu, Y. Zhang, J. Yan, A. R. Kahkoska, Z. Gu, Advances in bioresponsive closed-loop drug delivery systems. *Int. J. Pharm.* **544**, 350–357 (2018).
19. K. Y. Lin, J. H. Lo, N. Consul, G. A. Kwong, S. N. Bhatia, Self-titrating anticoagulant nanocomplexes that restore homeostatic regulation of the coagulation cascade. *ACS Nano* **8**, 8776–8785 (2014).
20. C. Li, H. Du, A. Yang, S. Jiang, Z. Li, D. Li, J. L. Brash, H. Chen, Thrombosis-responsive thrombolytic coating based on thrombin-degradable tissue plasminogen activator (t-PA) nanocapsules. *Adv. Funct. Mater.* **27**, 1703934 (2017).
21. Y. Zhang, J. Yu, J. Wang, N. J. Hanne, Z. Cui, C. Qian, C. Wang, H. Xin, J. H. Cole, C. M. Gallippi, Y. Zhu, Z. Gu, Thrombin-responsive transcutaneous patch for auto-anticoagulant regulation. *Adv. Mater.* **29**, 1604043 (2017).
22. A. T. Long, E. Kenne, R. Jung, T. A. Fuchs, T. Renné, Contact system revisited: An interface between inflammation, coagulation, and innate immunity. *J. Thromb. Haemost.* **14**, 427–437 (2016).
23. M. Levi, T. Keller, E. van Gorp, H. ten Cate, Infection and inflammation and the coagulation system. *Cardiovasc. Res.* **60**, 26–39 (2003).
24. M. Mittal, M. R. Siddiqui, K. Tran, S. P. Reddy, A. B. Malik, Reactive oxygen species in inflammation and tissue injury. *Antioxid. Redox Signal.* **20**, 1126–1167 (2014).
25. Y. Wang, L. Li, W. Zhao, Y. Dou, H. An, H. Tao, X. Xu, Y. Jia, S. Lu, J. Zhang, H. Hu, Targeted therapy of atherosclerosis by a broad-spectrum reactive oxygen species scavenging nanoparticle with intrinsic anti-inflammatory activity. *ACS Nano* **12**, 8943–8960 (2018).
26. K. S. Washington, C. A. Bashur, Delivery of antioxidant and anti-inflammatory agents for tissue engineered vascular grafts. *Front. Pharmacol.* **8**, 659 (2017).
27. J. T. Salonen, K. Nyyssönen, R. Salonen, H. M. Lakka, J. Kaikkonen, E. Porkkala-Sarataho, S. Voutilainen, T. A. Lakka, T. Rissanen, L. Leskinen, T. P. Tuomainen, V. P. Valkonen, U. Ristonmaa, H. E. Poulsen, Antioxidant Supplementation in Atherosclerosis Prevention (ASAP) study: A randomized trial of the effect of vitamins E and C on 3-year progression of carotid atherosclerosis. *J. Intern. Med.* **248**, 377–386 (2010).

28. C. Ping, Y. J. Sun, Z. C. Zhu, R. X. Wang, X. D. Shi, L. Chong, Y. T. Ye, A controlled release system of superoxide dismutase by electrospun fiber and its antioxidant activity in vitro. *J. Mater. Sci. Mater. Med.* **21**, 609–614 (2010).
29. J. D. Hayes, L. I. McLellan, Glutathione and glutathione-dependent enzymes represent a co-ordinately regulated defence against oxidative stress. *Free Radic. Res.* **31**, 273–300 (1999).
30. B. N. Singh, S. Shankar, R. K. Srivastava, Green tea catechin, epigallocatechin-3-gallate (EGCG): Mechanisms, perspectives and clinical applications. *Biochem. Pharmacol.* **82**, 1807–1821 (2011).
31. C. H. Kim, J. B. Mitchell, C. A. Bursill, A. L. Sowers, A. Thetford, J. A. Cook, D. M. van Reyk, M. J. Davies, The nitroxide radical TEMPOL prevents obesity, hyperlipidaemia, elevation of inflammatory cytokines, and modulates atherosclerotic plaque composition in apoE−/− mice. *Atherosclerosis* **240**, 234–241 (2015).
32. T. Reçber, İ. C. Haznedaroğlu, M. Çelebier, Review on characteristics and analytical methods of rivaroxaban. *Crit. Rev. Anal. Chem.* **2020**, 1–13 (2020).
33. D. K. Jagadeesha, T. E. Lindley, J. Deleon, R. V. Sharma, F. Miller, R. C. Bhalla, Tempol therapy attenuates medial smooth muscle cell apoptosis and neointima formation after balloon catheter injury in carotid artery of diabetic rats. *Am. J. Physiol. Heart Circ. Physiol.* **289**, H1047–H1053 (2005).
34. C. S. Wilcox, Effects of tempol and redox-cycling nitroxides in models of oxidative stress. *Pharmacol. Ther.* **126**, 119–145 (2010).
35. Y. Wang, B. Ma, A. Yin, B. Zhang, R. Luo, J. Pan, Y. Wang, Polycaprolactone vascular graft with epigallocatechin gallate embedded sandwiched layer-by-layer functionalization for enhanced antithrombogenicity and anti-inflammation. *J. Control. Release* **320**, 226–238 (2020).
36. Q. Y. Eng, P. V. Thanikachalam, S. Ramamurthy, Molecular understanding of Epigallocatechin gallate (EGCG) in cardiovascular and metabolic diseases. *J. Ethnopharmacol.* **210**, 296–310 (2018).
37. K. Qin, F. Wang, R. M. L. Simpson, X. Zheng, H. Wang, Y. Hu, Z. Gao, Q. Xu, Q. Zhao, Hyaluronan promotes the regeneration of vascular smooth muscle with potent contractile function in rapidly biodegradable vascular grafts. *Biomaterials* **257**, 120226 (2020).
38. H. S. Jung, W. H. Kong, D. K. Sung, M.-Y. Lee, S. E. Beack, D. H. Keum, K. S. Kim, S. H. Yun, S. K. Hahn, Nanographene oxide–hyaluronic acid conjugate for photothermal ablation therapy of skin cancer. *ACS Nano* **8**, 260–268 (2014).
39. Y. C. Hou, J. A. Li, S. J. Zhu, C. Cao, J. N. Tang, J. Y. Zhang, S. K. Guan, Tailoring of cardiovascular stent material surface by immobilizing exosomes for better pro-endothelialization function. *Colloids Surf. B Biointerfaces* **189**, 110831 (2020).
40. H. Jinnouchi, S. Torii, A. Sakamoto, F. D. Kolodgie, R. Virmani, A. V. Finn, Fully bioresorbable vascular scaffolds: Lessons learned and future directions. *Nat. Rev. Cardiol.* **16**, 286–304 (2019).
41. B. Zhang, Y. Su, J. Zhou, Y. Zheng, D. Zhu, Toward a better regeneration through implant-mediated immunomodulation: Harnessing the immune responses. *Adv. Sci.* **8**, e2100446 (2021).
42. E. Buck, S. Lee, L. S. Stone, M. Cerruti, Protein adsorption on surfaces functionalized with COOH groups promotes anti-inflammatory macrophage responses. *ACS Appl. Mater. Interfaces* **13**, 7021–7036 (2021).
43. Z. Yang, Y. Yang, L. Zhang, K. Xiong, X. Li, F. Zhang, J. Wang, X. Zhao, N. Huang, Mussel-inspired catalytic selenocystamine-dopamine coatings for long-term generation of therapeutic gas on cardiovascular stents. *Biomaterials* **178**, 1–10 (2018).
44. L. Li, L. Yang, Y. Liao, H. Yu, Z. Liang, B. Zhang, X. Lan, R. Luo, Y. Wang, Superhydrophilic versus normal polydopamine coating: A superior and robust platform for synergistic antibacterial and antithrombotic properties. *Chem. Eng. J.* **402**, 126196 (2020).
45. S. L. Goodman, Sheep, pig, and human platelet–material interactions with model cardiovascular biomaterials. *J. Biomed. Mater. Res.* **45**, 240–250 (1998).
46. R. C. Savani, G. Cao, P. M. Pooler, A. Zaman, Z. Zhou, H. M. DeLisser, Differential involvement of the hyaluronan (HA) receptors CD44 and receptor for HA-mediated motility in endothelial cell function and angiogenesis. *J. Biol. Chem.* **276**, 36770–36778 (2001).
47. P. Simon, M. T. Kasimir, G. Seebacher, G. Weigel, R. Ullrich, U. Salzer-Muhar, E. Rieder, E. Wolner, Early failure of the tissue engineered porcine heart valve SYNERGRAFT™ in pediatric patients. *Eur. J. Cardiothorac. Surg.* **23**, 1002–1006 (2003).
48. M. Arsalan, T. Walther, Durability of prostheses for transcatheter aortic valve implantation. *Nat. Rev. Cardiol.* **13**, 360–367 (2016).
49. S. Lin, X. Li, K. Wang, T. Shang, L. Zhou, L. Zhang, J. Wang, N. Huang, An albumin biopassive polyallylamine film with improved blood compatibility for metal devices. *Polymers* **11**, 734 (2019).
50. F. J. Schoen, R. J. Levy, Calcification of tissue heart valve substitutes: Progress toward understanding and prevention. *Ann. Thorac. Surg.* **79**, 1072–1080 (2005).
51. T. Shinoka, H. Miyachi, Current status of tissue engineering heart valve. *World J. Pediatr. Congenit. Heart Surg.* **7**, 677–684 (2016).
52. R. Levy, F. Schoen, J. Levy, A. C. Nelson, S. Howard, L. Oshry, Biologic determinants of dystrophic calcification and osteocalcin deposition in glutaraldehyde-preserved porcine aortic valve leaflets implanted subcutaneously in rats. *Am. J. Pathol.* **113**, 143–155 (1983).
53. G. Wright, J. Faught, J. Olin, Assessing anticalcification treatments in bioprosthetic tissue by using the New Zealand rabbit intramuscular model. *Comp. Med.* **59**, 266–271 (2009).
54. D. M. Martin, F. J. Boyle, Drug-eluting stents for coronary artery disease: A review. *Med. Eng. Phys.* **33**, 148–163 (2011).
55. H. Hashizume, P. Baluk, S. Morikawa, J. W. McLean, G. Thurston, S. Roberge, R. K. Jain, D. M. McDonald, Openings between defective endothelial cells explain tumor vessel leakiness. *Am. J. Pathol.* **156**, 1363–1380 (2000).
56. C. Atkinson, S. Stewart, P. D. Upton, R. Machado, J. R. Thomson, R. C. Trembath, N. W. Morrell, Primary pulmonary hypertension is associated with reduced pulmonary vascular expression of type II bone morphogenetic protein receptor. *Circulation* **105**, 1672–1678 (2002).
57. Y. Wang, Y. Lu, J. Zhang, X. Hu, Z. Yang, Y. Guo, Y. Wang, A synergistic antibacterial effect between terbium ions and reduced graphene oxide in a poly(vinyl alcohol)–alginate hydrogel for treating infected chronic wounds. *J. Mater. Chem. B* **7**, 538–547 (2019).
58. C. P. Regan, P. J. Adam, C. S. Madsen, G. K. Owens, Molecular mechanisms of decreased smooth muscle differentiation marker expression after vascular injury. *J. Clin. Invest.* **106**, 1139–1147 (2000).
59. D. W. Han, D. Y. Jung, J. C. Park, H. H. Cho, S. H. Hyon, D. K. Han, Underlying mechanism for suppression of vascular smooth muscle cells by green tea polyphenol EGCG released from biodegradable polymers for stent application. *J. Biomed. Mater. Res. A* **95**, 424–433 (2010).
60. F. Yang, H. He, L. Xu, L. Jin, G. Guo, Y. Wang, Inorganic-polymerization crosslinked tissue-siloxane hybrid as potential biomaterial for bioprosthetic heart valves. *J. Biomed. Mater. Res. Part A* **109**, 754–765 (2020).

Acknowledgments

Funding: This research was financially supported by the National Natural Science Foundation of China (32071357), Sichuan Science and Technology Program (2021YFH0011), National Key Research and Development Program (no. 2020YFC1107802), Chinese Academy of Medical Sciences (CAMS) Innovation Fund for Medical Sciences [CIFMS, (no. 2021-I2M-5-013)], 111 Project [The Program of Introducing Talents of Discipline to Universities (no. B16033)], Sichuan Science and Technology Major Project (no. 2018SZDZX0012), China Postdoctoral Science Foundation (2021 M692317), and National Natural Science Foundation of China (8210072669).

Author contributions: Conceptualization: Yanan Wang, R.L., and Yunbing Wang. Methodology: Yanan Wang, H.W., Z.Z., and K.L. Investigation: Yanan Wang, H.W., Z.Z., K.L., B.Z., L.Y., and R.L. Visualization: Yanan Wang, H.W., and Z.Z. Supervision: R.L. and Yunbing Wang. Writing—original draft: Yanan Wang. Writing—review and editing: M.F.M., R.L., and Yunbing Wang. **Competing interests:** The authors declare that they have no competing interests. **Data and materials availability:** All data needed to evaluate the conclusions in the paper are present in the paper and/or the Supplementary Materials.

Submitted 11 September 2021
Accepted 13 January 2022
Published 4 March 2022
10.1126/sciadv.abm3378

ScienceAdvances

A thrombin-triggered self-regulating anticoagulant strategy combined with anti-inflammatory capacity for blood-contacting implants

Yanan Wang, Haoshuang Wu, Zhongyi Zhou, Manfred F. Maitz, Kunpeng Liu, Bo Zhang, Li Yang, Rifang Luo, and Yunbing Wang

Sci. Adv., **8** (9), eabm3378.
DOI: 10.1126/sciadv.abm3378